Journal of Electroceramics (2020) 44:95–103
https://doi.org/10.1007/s10832-019-00195-2

Composition-insensitive enhanced piezoelectric properties in $SrZrO_3$ modified (K, Na)NbO_3-based lead-free ceramics

Jing Zhou[1] · Guanglei Xiang[1] · Jie Shen[1,2] · Huazhang Zhang[1] · Zhangmancang Xu[1] · Hang Li[1] · Peiyu Ma[1] · Wen Chen[1]

Received: 19 February 2019 / Accepted: 6 December 2019 / Published online: 14 December 2019

Abstract
In this work, composition-insensitive enhanced piezoelectric properties are achieved in (1-x)($K_{0.48}Na_{0.52}$)$_{0.96}Li_{0.04}$($Nb_{0.96}Sb_{0.04}$)O_3-$x$$SrZrO_3$ (KNN-SZ) lead-free ceramics. Rietveld refinements of the XRD patterns show that the introduction of $SrZrO_3$ straightens the O-B-O bond, leading to a relatively broad compositional region from $x = 0.04$ to 0.06 for the coexistence of orthorhombic-tetragonal (O-T) phase at room temperature. Within the phase coexistence region, relatively large and composition insensitive piezoelectric properties $d_{33} = 250 \sim 256$ pC/N and $k_p = 0.42 \sim 0.46$, as well as low dielectric loss tan $\delta = 0.026 \sim 0.028$ are attained in the KNN-SZ ceramics. The composition insensitivity of piezoelectric properties benefits from the enlarged ε_r and decreased P_r, which are originated from facilitated polarization rotation in the phase boundary region and normal ferroelectric-to-relaxor transition, respectively. Furthermore, an ultrahigh electric-field induced strain $S = 0.195\%$ is obtained, compared with reported KNN-based lead-free ceramics.

Keywords KNN-based lead-free piezoceramics · Composition-insensitivity · Piezoelectric properties · Phase transition · Ultrahigh strain

1 Introduction

Since Saito's milestone work of the high d_{33} of textured (K, Na)NbO_3 (KNN)-based ceramics in 2004 [1], an explosion of research on lead-free piezoelectric ceramics was ignited. Concerned with the complexity and cost of the templated grain growth (TGG) method, researchers put much effort in the pursuit of high d_{33} in nontextured KNN-based ceramics, and significant advances have been attained [2, 3]. Modification of phase boundaries is a common way to enhance the piezoelectric properties for both of lead-based and lead-free piezoceramics. Traditionally, there are two kinds of polymorphic phase transition (PPT) boundaries in KNN-based ceramics, i.e. orthorhombic-tetragonal (O-T) boundary and rhombohedral-orthorhombic (R-O) boundary, which are usually utilized in the development of ceramics with enhanced piezoelectric properties. However, their electrical properties are not high enough to be comparable to the lead-containing piezoceramics and to meet the requirements of practical applications [3]. Wu et al. proposed new phase boundary design idea, which eliminates the intermediate O phase to form a R-T phase boundary, and adjusted the $T_{R\text{-}T}$ closer to room temperature by introducing several additives in the KNN composition [4–8]. Based on the idea of new R-T phase boundary design, ultra-high piezoelectric coefficients d_{33} of 425 ~ 570 pC/N have been obtained. Besides small-signal piezoelectric properties, such as d_{33}, electric-field induced strain under an electric field of kilovolts order of magnitude, which is the key merit for actuator applications, is also reported to have been greatly improved for the KNN-based piezoceramics in recent years. Up to date, apart from piezoelectric properties, the main challenges that hinder extensive applications of these materials could be the process-related problems and the poor reproducibility [9, 10].

Concerning the poor reproducibility for the KNN-based piezoceramics, strong compositional dependence of piezoelectric properties is one of the main causes. Although the

✉ Jie Shen
shenjie@whut.edu.cn

[1] State Key Laboratory of Advanced Technology for Materials Synthesis and Processing, School of Materials Science and Engineering, Wuhan University of Technology, Wuhan 430070, People's Republic of China

[2] Engineering Research Center of Nano-Geo Materials of Ministry of Education, China University of Geosciences, Wuhan 430074, People's Republic of China

piezoelectric properties can be significantly enhanced by constructing R-T phase boundary, the narrow compositional range of reported R-T phase boundary leads the piezoelectric properties to have strong compositional dependence [4, 11]. For example, d_{33} quickly decays from the optimized composition, with only a 0.1% change in the composition of $(1-x-y)K_{1-w}Na_wNb_{1-z}Sb_zO_3$-$x$BiFeO$_3$-$yBi_{0.5}Na_{0.5}ZrO_3$ [12]. The heavy composition dependence and complex compositions involving eight or more elements will complicate large-scale production, where stable properties in simplified compositions are preferred [13].

Other scientific problems that need to be researched further are the mechanism of the boundary formation and the origin of ultrahigh d_{33} values. As declared in those publications [2, 3, 14], Zr^{4+} ion, as the B-site ion in perovskite structure, shifts $T_{R\text{-}O}$ up to the room temperature. Besides, many other researches on KNN-based ceramics show that introducing $AZrO_3$ (A = Ca, Sr, Ba) and $Bi_{1/2}(Na, K)_{1/2}ZrO_3$ lowers $T_{O\text{-}T}$ to room temperature and forms O-T boundary [15–19]. Therefore, it is still argued what the role of Zr^{4+} ion plays in the phase transition boundary adjusting. Recently, Yao et al. reported a diffused phase transition boundary in $CaZrO_3$ and MnO_2 co-modified (K, Na, Li)(Nb, Ta)O_3 ceramics with temperature-insensitive electric field-induced strains [18]. These results inspire us that understanding the effect of Zr^{4+} on the phase transition boundary may be the key to develop applicable KNN-based lead-free piezoelectric ceramics in a convenient low-cost way.

In this work, $(1\text{-}x)(K_{0.48}Na_{0.52})Li_{0.04}(Nb_{0.96}Sb_{0.04})O_3$-$x$SrZrO$_3$ ceramics (KNN-SZ, $x = 0 \sim 0.07$) were prepared and characterized to investigate the influence of $SrZrO_3$ on the O-T phase transition boundary. $SrZrO_3$ was selected as the additive with the considering of its suitable size (r_{Sr}^{2+} = 1.44 Å), which is closest to the average radius of A-site ions in KNN (r_A^+ = 1.48 Å, calculated from r_K^+ = 1.64 Å, r_{Na}^+ = 1.39 Å, and r_{Li}^+ = 0.92 Å) among the alkaline-earth metal cations' sizes (r_{Ca}^{2+} = 1.34 Å, r_{Ba}^{2+} = 1.61 Å) [20]. This would minimize the influence of the foreign A-site ion on the crystal structure. The coexistence of O-T phases at room temperature in the ceramics is obtained, and composition-insensitive enhanced piezoelectric properties are achieved in the O-T phase coexistence region. Effects of $SrZrO_3$ contents on the phase structure, crystal structure, and electrical properties of the KNN-SZ ceramics have been studied, and the relationships between structure and properties have been clearly illuminated.

2 Experimental

$(1\text{-}x)(K_{0.48}Na_{0.52})Li_{0.04}(Nb_{0.96}Sb_{0.04})O_3$-$x$SrZrO$_3$ ($x = 0 \sim 0.07$) ceramics were prepared by a conventional solid-state reaction method. Analytical grade raw materials powders of Na_2CO_3, K_2CO_3, Li_2CO_3, $SrCO_3$, Nb_2O_5, Sb_2O_3 and ZrO_2 were weighed, ball-milled, and then calcined at 850 ~ 880 °C for 4 h, depending on the content of SZ. The calcined powders were pressed into disks, and then sintered in the temperature range of 1100 ~ 1140 °C for 4 h. The crystal structure, morphology, and electrical properties for the KNN-SZ ceramics were characterized by the similar measurement procedures and apparatuses as those of our previous reported work on $Bi_{1/2}(Na_{0.8}K_{0.2})_{1/2}TiO_3$ lead-free ceramics [21].

3 Results and discussion

Figure 1 gives the relative density of the as-prepared samples. It shows that all the samples acquire relative density higher than 90%. FESEM images of the ceramics with different $SrZrO_3$ contents are presented in Fig. 2. Before observed by FESEM, the samples were thermally etched at 1070 ~ 1110 °C for 30 min. It is seen that the morphology of the samples are basically dense. For the sample with $x = 0$, the grain size is inhomogeneous. With x gradually increasing, the grain size gradually decreases and tends to be homogeneous. Finally, when x increases to 0.07, the grain size drops dramatically. The variation in grain size may be related to the fact that the incorporation of Zr^{4+} ions prohibits the grain growth and reduces grain size [11].

Figure 3 shows the XRD patterns of the KNN-SZ ceramics measured at room temperature. Standard XRD patterns for both O and T phases are also presented as references. From Fig. 3(a), perovskite phase is observed in all the samples. Figure 3(b) shows the XRD profiles in the 2θ range of 44.5 ~ 46.5°. It can be seen that the (200) peak gradually shifts to low angle side. In the consideration of the average A-site ion radius of r_A^+ = 1.48 Å, the change of the crystal structure by introducing Sr^{2+} (r_{Sr}^{2+} = 1.44 Å) at the A-site would be negligible. However, the substitution of Nb^{5+} (r_{Nb}^{5+} = 0.64 Å) by

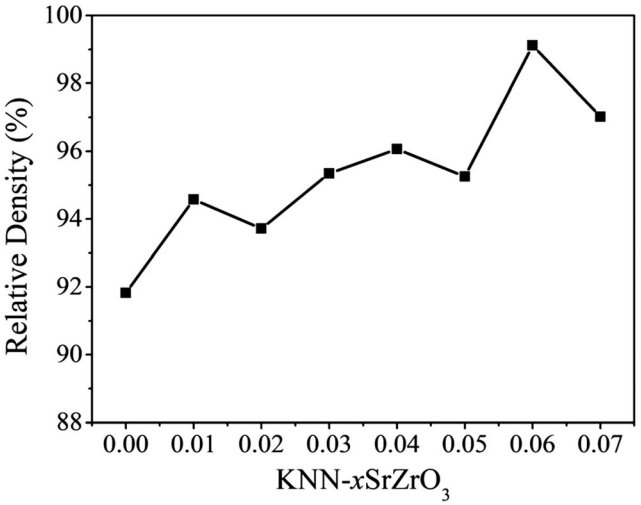

Fig. 1 Relative density of the as-prepared KNN-xSZ ceramic samples

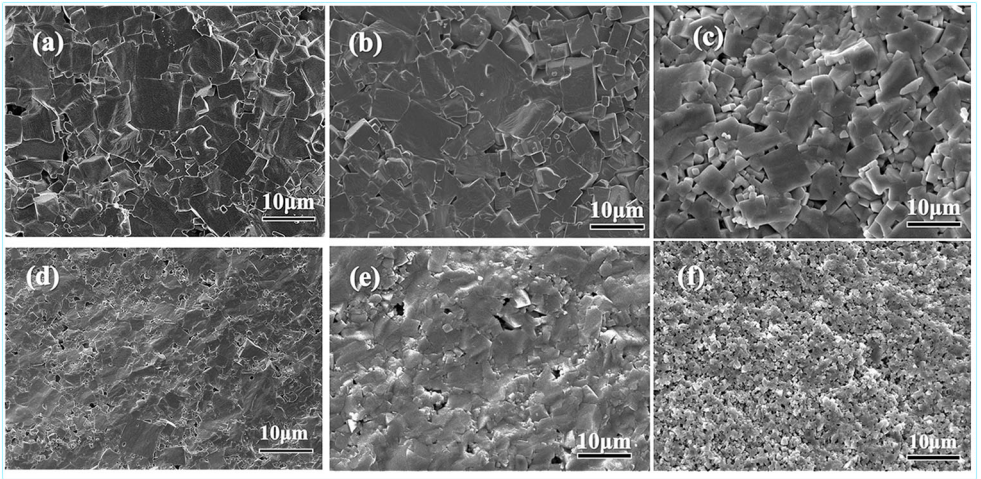

Fig. 2 FESEM images of thermal etched cross-section for KNN-*x*SZ ceramics with different *x* contents: (**a**) $x = 0$; (**b**) $x = 0.03$; (**c**) $x = 0.04$; (**d**) $x = 0.05$; (**e**) $x = 0.06$; (**f**) $x = 0.07$

Zr^{4+} ($r_{Zr}^{4+} = 0.72$ Å) on the B-site may enlarge the unit cell, which induces the shift of the $(200)_{pc}$ peak ("pc" is short for "pseudocubic") towards low angles [22]. For KNN-based ceramics with randomly oriented grains, the phase structure could be determined by the relative intensity of the reflections $(002)_{pc}/(200)_{pc}$ ($I_{(002)}/I_{(200)}$) [23]. The $I_{(002)}/I_{(200)}$ value of 2:1 is the indication of O phase, while the $I_{(002)}/I_{(200)}$ value of 1:2 suggests that the sample is predominately in T phase. It can be seen that when *x* is 0, the $I_{(002)}/I_{(200)}$ ratio is approximately 2:1, suggesting the existence of O phase. With *x* going up, the peak intensity of $(200)_{pc}$ crystal plane increases, indicating that T phase appears and its proportion gradually increases. O-T coexistence is obtained in the composition range of $0.04 \le x \le 0.06$, where the $I_{(002)}/I_{(200)}$ value is close to 1. When *x* value further increases to 0.07, only one diffraction peak is observed, suggesting the pseudo-cubic phase. The XRD results show that the introduction of $SrZrO_3$ leads to the O-T phases coexistence, i.e. the polymorphic O-T phase transition boundary, in a wide composition range, from $x = 0.04$ to $x = 0.06$.

To determine the phase contents, Rietveld refinement of XRD patterns is performed by the Maud program based on about 20 diffraction peaks [11, 24, 25]. Space groups of *A*mm2 (ICSD-9533) and *P*4mm (ICSD-9532) are chosen as the initial models for orthorhombic and tetragonal phases, respectively. The calculated patterns are in good agreement with the experimental data, with $R_{wp} = 15.7\%$, $sig = 1.41$ for $x = 0.04$, and $R_{wp} = 11.7\%$, $sig = 1.24$ for $x = 0.06$, respectively. As shown in Table 1, the refinement results show that with *x* increasing from 0.04 to 0.06, changes in proportions of O and T phases are quite small (only about 6%). This suggests that in the composition range of O-T phase boundary, the dependence of phase structure on the ceramic composition is

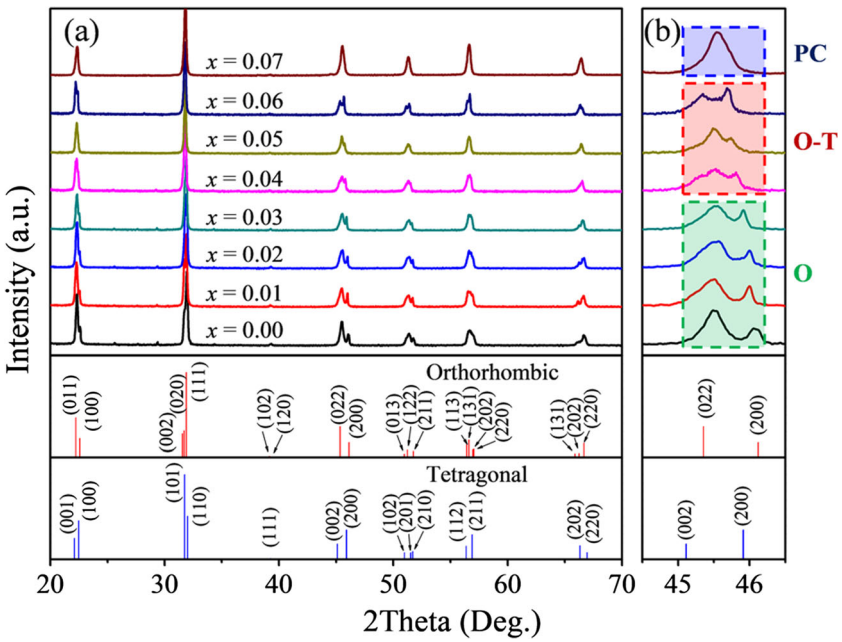

Fig. 3 XRD patterns of KNN-*x*SZ ceramics: (**a**) $2\theta = 20 \sim 80°$, (b) $2\theta = 44.5 \sim 46.5°$. Standard XRD patterns for both orthorhombic and tetragonal phases are presented at the bottom as references

Table 1 Results of Rietveld refinement for the crystal structures and lattice parameters of KNN-xSrZrO$_3$ ceramics with $x = 0.04$ and $x = 0.06$

Parameters	$x = 0.04$		$x = 0.06$	
sig	1.41		1.24	
R_{wp} (%)	15.7		11.7	
Phase	O	T	O	T
Volume fraction (%)	68.34	31.66	62.16	37.84
a (Å)	3.9578	3.9845	3.9561	3.9845
b (Å)	5.6421	3.9845	5.6441	3.9845
c (Å)	5.6470	3.9621	5.6517	3.9642
Cell volume (V)	126.10	62.90	126.20	63.93
c/*a* ratio	1.4268	0.9943	1.4286	0.9949
Beta (deg)	90	90	90	90
Atomic positions				
A atomic (*x, y, z*)	0.5; 0; 0.4933	0; 0; 0.0436	0.0007; 0; −0.0054	0; 0; 0.0401
B atomic (*x, y, z*)	−1.0005; 0; −0.0080	0.5; 0.5; 0.4768	0.5; 0; 0.4986	0.5; 0.5; 0.4833
O1 atomic (*x, y, z*)	0.5; 0; 0.0272	0.5; 0.5; 0.0567	0.5; 0; 0.0361	0.5; 0.5; 0.04900
O2 atomic (*x, y, z*)	0; 0.2260; 0.2939	0.5; 0; 0.4742	0; 0.2287; 0.2903	0.5; 0; 0.4687

non-pronounced. Consequently, the polymorphic O-T phase boundary of the KNN-SZ ceramics is expected to exhibit weak compositionally dependent electrical properties.

Based on the Rietveld refinement, the oxygen octahedral distortion and polarization vectors of the ceramics for $x = 0.04$ and $x = 0.06$ are shown in Fig. 4. Oxygen octahedron parameters are listed in Table 2. From the aspect of the tetragonal phase, the distortion degree of the oxygen octahedron decreases with the increasing of x, as shown in Fig. 4(b, f). Moreover, the *c*/*a* ratios are 0.9943 and 0.9950 for $x = 0.04$ and $x = 0.06$, respectively. The increase of *c*/*a* ratio towards 1 implies a tendency of structural change from tetragonal to pseudo-cubic. In the view of the oxygen octahedral distortion of the orthorhombic phase, the sample with $x = 0.06$ has a smaller torsion angle than the sample with $x = 0.04$, as shown in Fig. 4(c, g), i.e. the covalent bond of O-B-O is straightened with the increase of x. This indicates that the introduction of $SrZrO_3$ weakens the distortion of oxygen octahedron, which causes the reduction of transition barrier between O and T phases. Furthermore, the straight -[BO_6]- chain has a low tendency for ordering, which may lead to more local order-disorder of the structure in the ceramics.

To clarify the detail of the phase transition process in the KNN-SZ ceramics, in situ temperature dependent XRD measurements for $x = 0.04$ and $x = 0.06$ ceramics were carried out in the temperature range of 25 ~ 300 °C and 25 ~ 240 °C, respectively. The results are shown in Fig. 5. For comparison purpose, the temperature dependent dielectric constant of both compositions is also shown in Fig. 5. As shown in Fig. 5(a), O-T phases coexist in the ceramic with $x = 0.04$ in the temperature range from 25 °C to 80 °C. In this range, the peak intensity of (200) crystal plane increases with temperature, implying the O to T phase transition. With the temperature further increasing above 100 °C, the value of $I_{(002)}/I_{(200)}$ increases to about 2 until the temperature of 200 °C, suggesting that T phase is dominant from 100 °C to 200 °C. Finally, above the temperature of 240 °C, (002) and (200) peaks converge together and merge into one single peak, showing that the sample is in cubic phase above 240 °C. As plotted in Fig. 5(b), the temperature dependent dielectric constant (ε_r-T curve) agrees well to the structural transition revealed by in situ XRD patterns. It clearly illustrates the relationship between the anomaly of dielectric constant and the evolution of (002)/(200) peaks. Analogically, the phase structure evolution of the ceramic with $x = 0.06$ is clarified in the same way. As shown in Fig. 5(c, d), O-T coexists at 25 ~ 80 °C, while the stable T phase and cubic phase are obtained at 100 ~ 160 °C and above 200 °C, respectively. Comparing the ε_r-T curves of the two compositions, it can be observed that diffuseness of the O-T transition gradually becomes more pronounced with the increase of $SrZrO_3$ amount. These results indicate that $SrZrO_3$ doping makes the ceramics acquire a more relaxor-like character, which is similar to Yao's results for the KNN-CZ ($CaZrO_3$) ceramics [18].

Figure 6(a) plots the temperature dependent dielectric constant of all the KNN-SZ samples at 100 kHz, to reveal the composition induced crossover from normal ferroelectric to relaxor in the KNN-SZ system. It is seen that T_C decreases from 353 °C to 182 °C with x increasing from 0 to 0.06, and the peak at T_C becomes highly diffused with x up to 0.07 and the diffused peaks are observed. Moreover, $T_{O\text{-}T}$ drops gradually with x going up to 0.06, and a wide temperature range of the phase transition from 20 to 60 °C is found when x value changes from 0.04 to 0.06. To better show the evolution of phase transition temperatures, the temperature dependent dielectric constant

from about −100 °C to 150 °C was also measured. The results are presented in Fig. 6(b). From this figure, it is further confirmed that $T_{O\text{-}T}$ decreases continuously with the increase of $SrZrO_3$ content, whereas the rhombohedral to orthorhombic transition temperature $T_{R\text{-}O}$ cannot be identified. The reductions in both T_C and $T_{O\text{-}T}$ are consistent with previous reports [15–18]. The diffused O-T phase transition and decreased $T_{O\text{-}T}$ lead to the O-T coexistence in the composition range from $x = 0.04$ to 0.06 at room temperature.

As shown in Fig. 6(c), the ε_r-T curves of the ceramic with $x = 0.05$ exhibit frequency dispersion in the range of 100 Hz ~ 100 kHz and the peak at T_C shifts to high temperature with the frequency increasing, which is the characteristic of the relaxor ferroelectrics. To characterize the relaxor behavior of the ceramics, temperature dependent dielectric property is analyzed in terms of the modified Curie-Weiss law [26]:

$$\frac{1}{\varepsilon_r}-\frac{1}{\varepsilon_m}=\frac{(T-T_m)^\gamma}{C},\quad 1\le\gamma\le 2 \tag{1}$$

where ε_m is the maximum value of ε_r at T_m, C is the Curie constant, and the γ parameter represents the diffuseness degree value between 1 and 2. The boundary value of $\gamma = 1$ indicates that the ceramic is normal ferroelectrics, while the other boundary value of $\gamma = 2$ is a typical characteristic for ideal relaxor ferroelectrics [27]. The values of γ is obtained by fitting $\ln(1/\varepsilon\text{-}1/\varepsilon_m)$ as a function of $\ln(T\text{-}T_m)$ as shown in Fig. 6(d-i). The results show that with x increasing from 0 to 0.07, the values of γ change from 1.465 to 1.795, indicating the composition induced a normal ferroelectric-to-relaxor transformation.

Figure 7(a) shows the *P-E* hysteresis loops of the KNN-SZ ceramics with different SZ contents measured at 1 Hz and 30 °C. A saturated and square-shaped *P-E* loop, which is a typical characteristic of normal ferroelectrics, is achieved for the ceramic sample with $x = 0$. With x increasing, the *P-E* loops become slender, which confirms the composition induced a normal ferroelectric-to-relaxor transformation. To clearly show the variations in ferroelectric properties, remnant polarization (P_r) and coercive field (E_C) as functions of SZ content are presented in Fig. 7(b). With x increasing, $2P_r$ drops continuously while $2E_c$ only drops obviously in the range from $x = 0.03$ to 0.06. The dropping of P_r is related to the above-mentioned normal ferroelectric-to-relaxor transformation. It is believed that the relaxation behavior originates from the local order-disorder of the structure and the formation of polar nano-regions (PNRs), which weakens the ferroelectricity and lowers P_r [26]. At the meantime, in the phase boundary region, the O-T phases coexistence provides more polarization vectors, which facilitates domain switching and polarization reversal under the external electric field [28], leading to the lineally dropping of E_c in this range.

Table 2 Oxygen octahedron parameters of KNN-xSrZrO$_3$ ceramics with $x = 0.04$ and $x = 0.06$

Parameters	$x = 0.04$		$x = 0.06$	
	P4mm	*Amm2*	*P4mm*	*Amm2*
Nb-O_{1A} (Å)	2.2977	1.9909	2.2427	1.9945
Nb-O_{1B} (Å)	1.6645	1.9869	1.7215	1.9892
Nb-O_{2A} (Å)	1.9923	1.9082	1.9931	2.1115
Nb-O_{2B} (Å)	1.9923	2.1291	1.9931	1.9179
Nb-O_{2C} (Å)	1.9923	2.1291	1.9931	1.9179
Nb-O_{2D} (Å)	1.9923	1.9082	1.9931	2.1115
∠O_{1A}-Nb-O_{1B} (°)	180	168.515	180	166.499
∠O_{2A}-Nb-O_{2C} (°)	180	162.663	176.673	164.709
∠O_{2B}-Nb-O_{2D} (°)	180	162.663	176.673	164.709

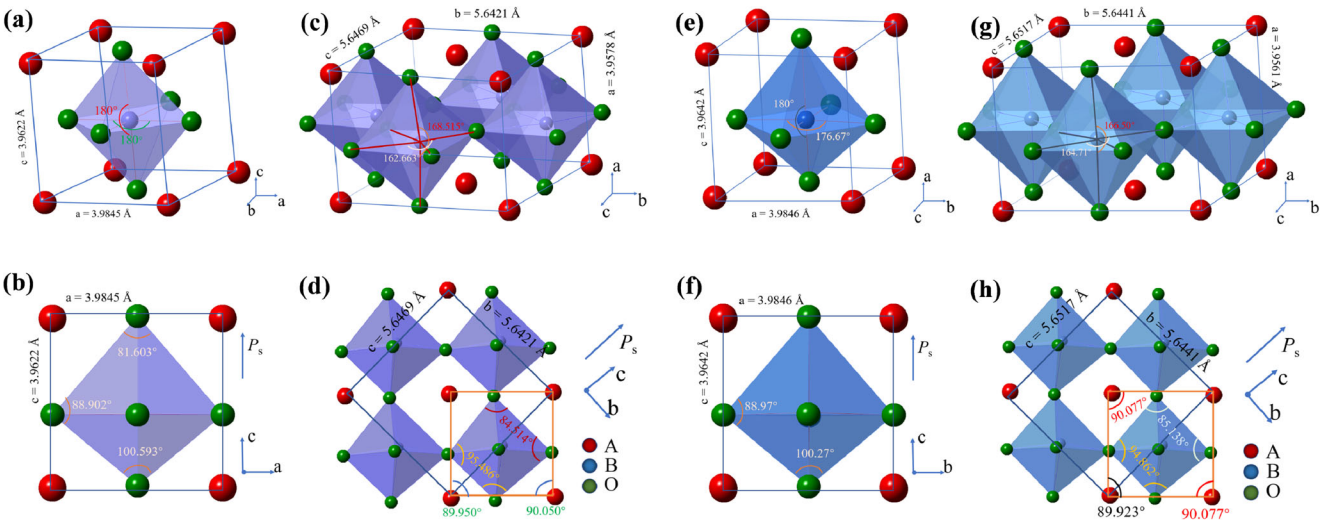

Fig. 4 Crystal structure of the ceramics to illustrate the distortion of the oxygen octahedron: (**a**, **b**) T phase and (**c**, **d**) O phase for $x = 0.04$; (**e**, **f**) T phase and (**g**, **h**) O phase for $x = 0.06$

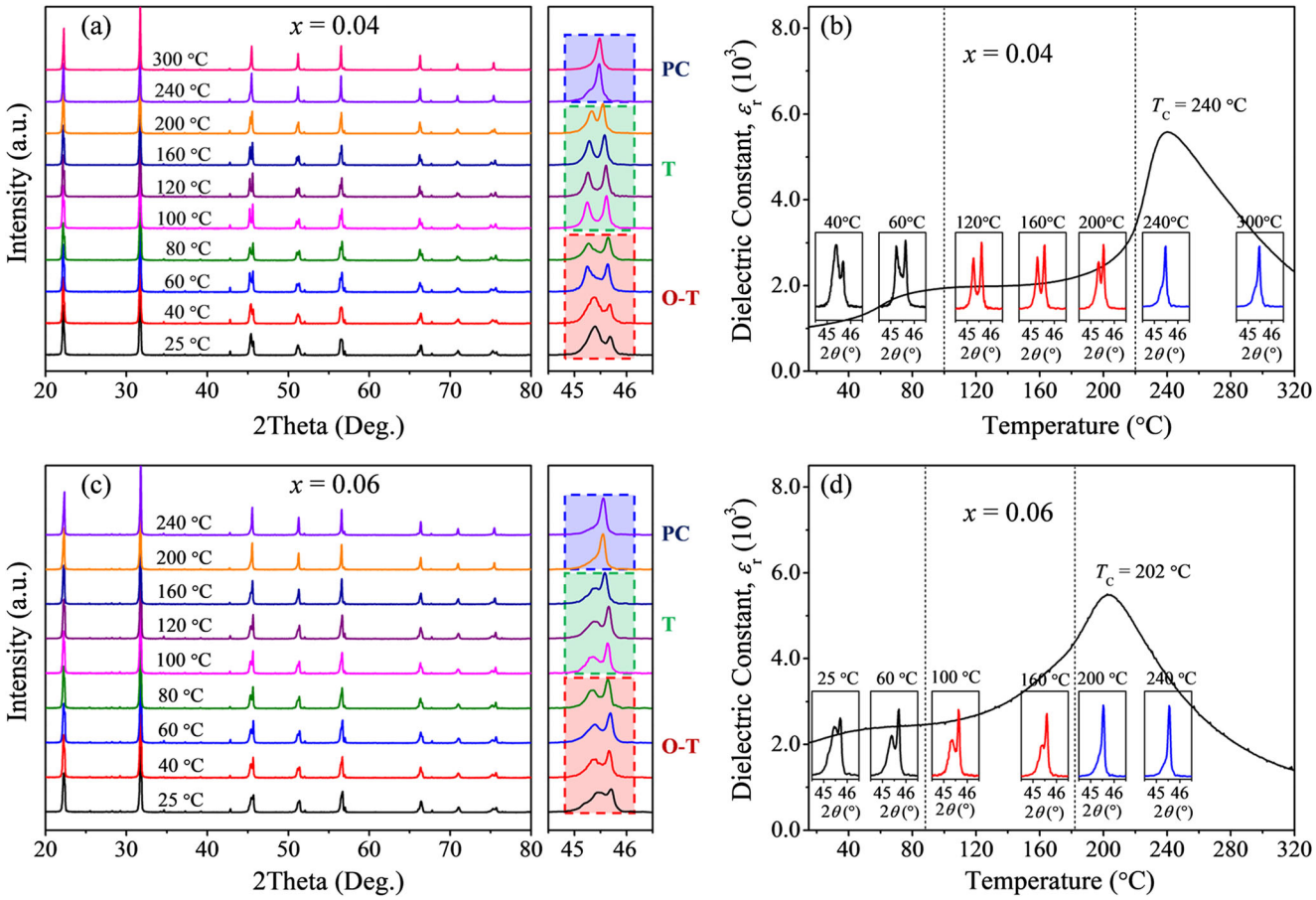

Fig. 5 In situ temperature dependent XRD patterns, and the comparisons between the temperature dependent dielectric constant and the evolution of XRD profile for the KNN-*x*SZ ceramics with (**a**, **b**) $x = 0.04$ and (**c**, **d**) $x = 0.06$

Figure 7(c) presents the electromechanical coupling factor k_p and the maximal phase angle θ_{max} of the lowest planar mode of disc-shaped samples. The inset figure in Fig. 7(c) shows the definition of θ_{max}. Usually, θ_{max} is regarded as a measure of poling degree, and a piezoceramic could be considered to be fully poled when its θ_{max} approximates to 90° [16, 27]. As shown in Fig. 7(c), relatively high θ_{max} values are achieved with $x = 0 \sim 0.06$, indicating that these samples are nearly fully poled. The variation of piezoelectric constant d_{33} with the addition of SZ is shown in Fig. 7(b). It can be seen that the d_{33} increases initially and then decreases with the SZ content increasing. A plateau of $d_{33} = 250 \sim 256$ pC/N with $k_p = 0.42 \sim 0.46$ is observed in a wide compositional range of $0.04 \le x \le 0.06$, i.e. the variations of the piezoelectric properties are minor in the O-T phase boundary region. This composition insensitivity means that the ceramics can be easily controlled in mass production to gain the expected piezoelectric performances, compared with previous reports [11, 12]. The improvement of piezoelectric properties could benefit from the low energy barriers between O and T phases, which facilitate the polarization rotation and domain wall movement near the polymorphic phase boundary [4, 8]. Furthermore, when x increases to 0.07, d_{33} drops dramatically, which results from the small grain size of the sintered ceramics and the appearance of pseudo-cubic phase. An empirical formula is employed to illuminate the physical mechanisms of the enhanced d_{33}, which is connected with the enhanced dielectric and ferroelectric properties (e.g. $d_{33} \sim 2\alpha P_r \varepsilon_r$). The comparison on variations of d_{33} and $2P_r \times \varepsilon_r$ with $SrZrO_3$ content is shown in Fig. 7(d). It shows that variation trends of d_{33} and $2P_r \times \varepsilon_r$ are quite similar. The variation of ε_r with $SrZrO_3$ content is shown in the inset figure in Fig. 7(d). Different from the continuously decreasing tendency of $2P_r$, the value of ε_r is enlarged by the facilitated polarization in the phase boundary region, due to the same reason of the decrease of E_c. By this enhanced dielectric property, the enhanced piezoelectric properties are obtained in the phase boundary region, although the ferroelectric property, P_r, decreases continuously with doping. Furthermore, synergy of the enlarged ε_r and decreased P_r leads to composition insensitivity of the piezoelectric properties of the KNN-SZ ceramics, which is preferred for large-scale production.

Figure 8(a, b) shows the unipolar electric-field induced strains and normalized large-signal piezoelectric coefficient

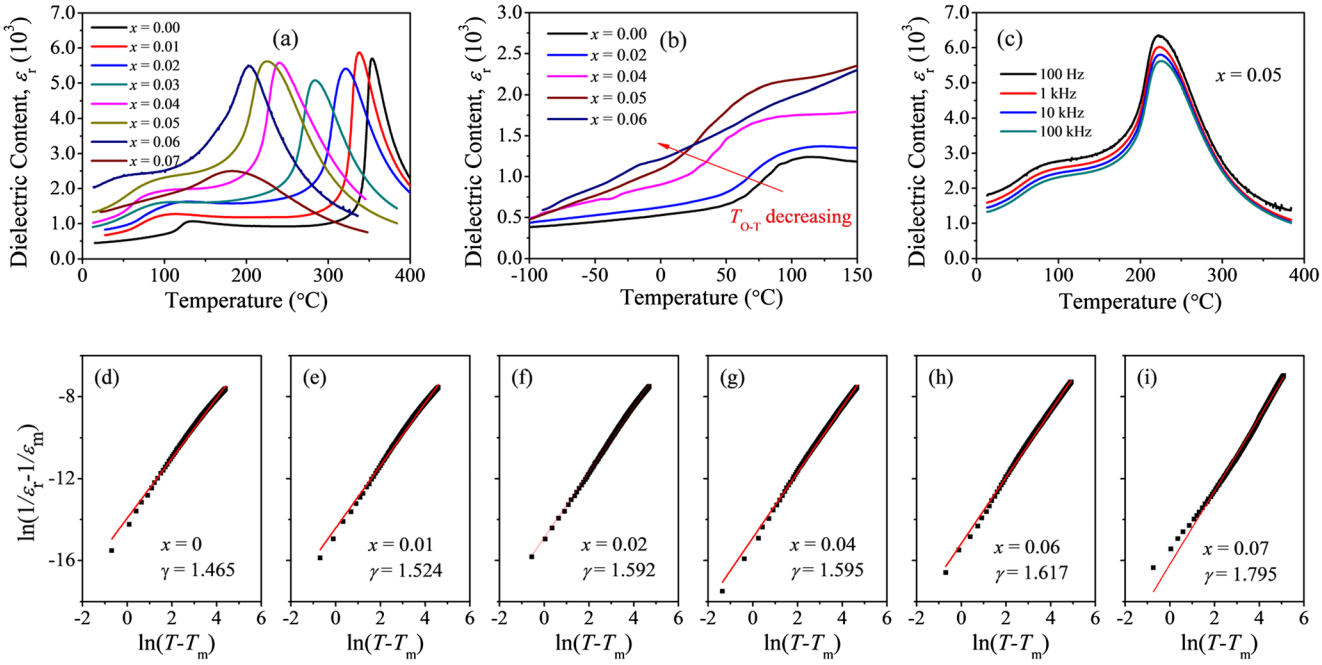

Fig. 6 Temperature dependent dielectric constant of KNN-xSZ ceramics: (**a**) ε_r -T curves of KNN-xSZ ceramics with different x values from 0 ~ 400 °C; (**b**) ε_r -T curves of KNN-xSZ ceramics with different x values from −100 ~ 150 °C; (**c**) temperature dependent dielectric constant at different frequencies (100 ~ 100 kHz) for KNN-0.05SZ; (**d-i**) inverse dielectric permittivity at 100 kHz as a function of temperature for KNN-xSZ ceramics with different x values

$d_{33}{}^*$ (S_{max}/E_{max}) of the KNN-xSZ ceramics with the variation of x at 1 Hz, respectively. The strain curves of all samples exhibit basically linear strain response, which is suitable for the device design. The strain values at 4 kV/mm for the ceramics increase with the x increasing. Particularly, an ultrahigh electric-field induced strain $S = 0.195\%$ is achieved with the composition x of 0.06, which is superior to many reports [15, 29–31] (as compared in Fig. 7(b, c)). This outstanding performance is due to the above-mentioned reduced barrier between O and T phases, which favors the domain switching and domain wall movement under an electric field. The ultrahigh strain and basically linear strain response of the KNN-xSZ ($x = 0.6$) ceramic give it an attractive potential in actuator application.

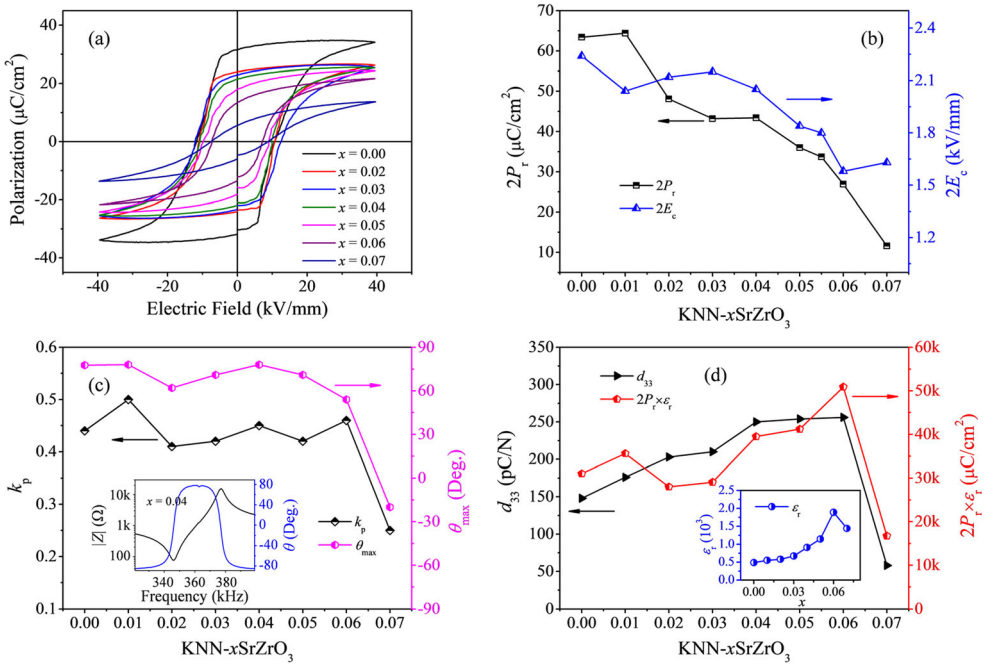

Fig. 7 Ferroelectric and piezoelectric properties of KNN-xSZ ceramics. (**a**) P-E loops of KNN-xSZ ceramics; (**b**) $2P_r$ and $2E_c$ as functions of x contents; (**c**) electromechanical coupling factor k_p and the maximal phase angle θ_{max} of KNN-xSZ ceramics, with an inset figure showing the impedance spectrum near the resonance frequency of the lowest planar mode of the disc-shaped sample; (**d**) comparison of the variation trends of ε_r and $2P_r \times \varepsilon_r$ with x contents; the inset figure in (**d**) shows the variation of ε_r with $SrZrO_3$ content

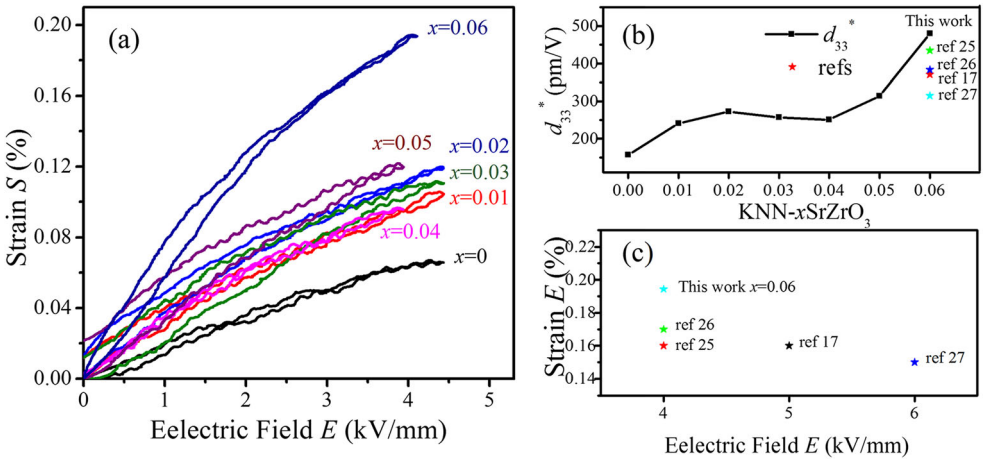

Fig. 8 (**a**)Unipolar electric field-induced strains of the KNN-*x*SZ ceramics at 1 Hz. (**b**) normalized d_{33}^* for KNN-*x*SZ and several works on KNN-based ceramics; (**c**) unipolar strains for KNN-0.06SZ ceramic and several other works on KNN-based ceramic systems, which were selected at room temperature in the contexts

4 Conclusions

The effect of $SrZrO_3$ modification on the structure and electric properties of KNN-based lead-free ceramics is investigated. It is found that the introduction of $SrZrO_3$ straightens the O-B-O bond, reduces the O-T phases transition barrier, and promotes structure disordering in the ceramics. The reduced O-T phases transition barrier lowers down $T_{O\text{-}T}$ to room temperature. Consequently, O-T phase coexistence region is obtained at room temperature within a relatively broad composition range from $x = 0.04$ to 0.06. In this phase boundary region, ε_r is enlarged because of the facilitated polarization rotation. In the meantime, more structural disorder makes the ceramics transit from normal ferroelectrics to relaxor, leading to P_r decreasing. As a result of synergy of enlarged ε_r and decreased P_r, composition-insensitive enhanced piezoelectric properties are attained in the phase boundary region. Furthermore, an outstanding electric-field induced strain performance has also been found in the KNN-based lead-free ceramics, providing an attractive potential in actuator application.

Acknowledgements This work was financially supported by the National Natural Science Foundation of China (No. 51572205), the Equipment Pre-Research Joint Fund of EDD and MOE (No. 6141A02022262), the open project of Engineering Research Center of Nano-Geo Materials of Ministry of Education (NGM2019KF005), the Fundamental Research Funds for the Central Universities (WUT: 2017III035, 2018III019).

References

1. Y. Saito, H. Takao, T. Tani, T. Nonoyama, K. Takatori, T. Homma, T. Nagaya, M. Nakamura, Lead-free piezoceramics. Nature **432**, 84–87 (2004)
2. T. Zheng, J. Wu, D. Xiao, J. Zhu, Recent development in lead-free perovskite piezoelectric bulk materials. Prog. Mater. Sci. **98**, 552–624 (2018)
3. J. Wu, D. Xiao, J. Zhu, Potassium–sodium niobate lead-free piezoelectric materials: Past, present, and future of phase boundaries. Chem. Rev. **115**, 2559–2595 (2015)
4. B. Zhang, J. Wu, X. Cheng, X. Wang, D. Xiao, X. Wang, X. Lou, Lead-free piezoelectrics based on potassium–sodium niobate with giant d_{33}. ACS Applied Materials & Interfaces **5**, 7718–7725 (2013)
5. H. Tao, J. Wu, Giant piezoelectric effect and high strain response in $(1-x)(K_{0.45}Na_{0.55})(Nb_{1-y}Sb_y)O_3$-$xBi_{0.5}Na_{0.5}Zr_{1-z}HfzO_3$ lead-free ceramics. J. Eur. Ceram. Soc. **36**, 1605–1612 (2016)
6. J. Wu, X. Wang, X. Cheng, T. Zheng, B. Zhang, D. Xiao, J. Zhu, X. Lou, New potassium-sodium niobate lead-free piezoceramic: Giant-d_{33} vs. sintering temperature. Journal of Applied Physics **115**, 114104 (2014)
7. K. Xu, J. Li, X. Lv, J. Wu, X. Zhang, D. Xiao, J. Zhu, Superior piezoelectric properties in potassium–sodium niobate lead-free ceramics. Adv. Mater. **28**(38), 8519–8523 (2016)
8. T. Zheng, H. Wu, Y. Yuan, X. Lv, Q. Li, T. Men, C. Zhao, D. Xiao, J. Wu, K. Wang, J.-F. Li, Y. Gu, J. Zhu, S.J. Pennycook, The structural origin of enhanced piezoelectric performance and stability in lead free ceramics. Energy Environ. Sci. **10**, 528–537 (2017)
9. K. Wang, B. Malič, J. Wu, Shifting the phase boundary: Potassium sodium niobate derivates. MRS Bull. **43**, 607–611 (2018)
10. H.-C. Thong, C. Zhao, Z. Zhou, C.-F. Wu, Y.-X. Liu, Z.-Z. Du, J.-F. Li, Wen Gong, Ke Wang, technology transfer of lead-free (K, Na)NbO_3-based piezoelectric ceramics. Mater. Today (2019). https://doi.org/10.1016/j.mattod.2019.04.016
11. L. Jiang, Y. Li, J. Xing, J. Wu, Q. Chen, H. Liu, D. Xiao, J. Zhu, Phase structure and enhanced piezoelectric properties in $(1-x)(K_{0.48}Na_{0.52})(Nb_{0.95}Sb_{0.05})O_3$-$x(Bi_{0.5}Na_{0.42}Li_{0.08})_{0.9}Sr_{0.1}ZrO_3$ lead-free piezoelectric ceramics. Ceram. Int. **43**, 2100–2106 (2017)
12. B. Wu, H. Wu, J. Wu, D. Xiao, J. Zhu, S.J. Pennycook, Giant piezoelectricity and high curie temperature in nanostructured alkali niobate lead-free piezoceramics through phase coexistence. J. Am. Chem. Soc. **138**(47), 15459–15464 (2016)
13. S. Trolier-McKinstry, S. Zhang, A.J. Bell, X. Tan, High-performance piezoelectric crystals, ceramics, and films. Annu. Rev. Mater. Res. **48**, 191–127 (2018)
14. R. Wang, H. Bando, T. Katsumata, Y. Inaguma, H. Taniguchi, M. Itoh, Tuning the orthorhombic-rhombohedral phase transition temperature in sodium potassium niobate by incorporating barium zirconate. Phys. Status Solidi RRL **3**, 142–144 (2009)
15. Y. Qin, J. Zhang, W. Yao, C. Lu, S. Zhang, Domain configuration and thermal stability of $(K_{0.48}Na_{0.52})(Nb_{0.96}Sb_{0.04})O_3$–$Bi_{0.50}(Na_{0.82}K_{0.18})_{0.50}ZrO_3$ piezoceramics with high d_{33} coefficient. ACS Appl. Mater. Interfaces **8**, 7257–7265 (2016)
16. Y. Zhang, L. Li, B. Shen, J. Zhai, Effect of orthorhombic-tetragonal phase transition on structure and piezoelectric properties of KNN-based lead-free ceramics. Dalton Trans. **44**, 7797–7802 (2015)

17. Q. Li, M.-H. Zhang, Z.-X. Zhu, K. Wang, J.-S. Zhou, F.-Z. Yao, J.-F. Li, Poling engineering of (K,Na)NbO_3-based lead-free piezoceramics with orthorhombic-tetragonal coexisting phases. J. Mater. Chem. C **5**, 549–556 (2017)
18. F.-Z. Yao, K. Wang, W. Jo, K.G. Webber, T.P. Comyn, J.-X. Ding, B. Xu, L.-Q. Cheng, M.-P. Zheng, Y.-D. Hou, J.-F. Li, Diffused phase transition boosts thermal stability of high-performance lead-free piezoelectrics. Adv. Funct. Mater. **26**, 1217–1224 (2016)
19. X. Wang, J. Wu, D. Xiao, J. Zhu, X. Cheng, T. Zheng, B. Zhang, X. Lou, X. Wang, Giant piezoelectricity in potassium-sodium niobate lead-free ceramics. J. Am. Chem. Soc. **136**(7), 2905–2910 (2014)
20. R. Shannon, Revised effective ionic radii and systematic studies of interatomic distances in halides and chalcogenides. Acta Crystallographica Section A **32**, 751–767 (1976)
21. H. Zhang, J. Zhou, J. Shen, X. Yang, C.-L. Wu, K.-K. Han, Z.-H. Zhao, W. Chen, Enhanced piezoelectric property and promoted depolarization temperature in Fe doped $Bi_{1/2}(Na_{0.8}K_{0.2})_{1/2}TiO_3$ lead-free ceramics. Ceram. Int. **43**, 16395–16402 (2017)
22. X. Lv, Z. Li, J. Wu, J. Xi, M. Gong, D. Xiao, J. Zhu, Enhanced piezoelectric properties in potassium-sodium niobate-based ternary ceramics. Mater. Des. **109**, 609–614 (2016)
23. J. Fu, R. Zuo, Y. Xu, J.-F. Li, M. Shi, Investigations of domain switching and lattice strains in (Na,K)NbO_3-based lead-free ceramics across orthorhombic-tetragonal phase boundary. J. Eur. Ceram. Soc. **37**, 975–983 (2017)
24. M.H. Jiang, G.Q. Zhao, Z.F. Gu, G. Cheng, X.Y. Liu, L. Li, Y.S. Du, In-depth structure characterization and properties of $(1-x)(Li_{0.05}Na_{0.475}K_{0.475})(Nb_{0.95}Sb_{0.05})O_3$-$x$$BiFeO_3$ lead-free piezoceramics. J. Mater. Sci. Mater. Electron. **26**, 9366–9372 (2015)
25. X. Lv, J. Wu, D. Xiao, J. Zhu, X. Zhang, Structural evolution of the R-T phase boundary in KNN-based ceramics. J. Am. Ceram. Soc. **101**, 1191–1200 (2018)
26. R. Zuo, J. Fu, S. Lu, Z. Xu, Normal to relaxor ferroelectric transition and domain morphology evolution in (K,Na)(Nb,Sb)O_3-$LiTaO_3$-$BaZrO_3$ lead-free ceramics. J. Am. Ceram. Soc. **94**, 4352–4357 (2011)
27. T. Takenaka, H. Nagata, Y. Hiruma, Y. Yoshii, K. Matumoto, Lead-free piezoelectric ceramics based on perovskite structures. J. Electroceram. **19**, 259–265 (2007)
28. B. Liu, Y. Zhang, P. Li, B. Shen, J. Zhai, Phase transition and electrical properties of $Bi_{0.5}(Na_{0.8}K_{0.2})_{0.5}ZrO_3$ modified $(K_{0.52}Na_{0.48})(Nb_{0.95}Sb_{0.05})O_3$ lead-free piezoelectric ceramics. Ceram. Int. **42**, 13824–13829 (2016)
29. M.-H. Zhang, K. Wang, J.-S. Zhou, J.-J. Zhou, X. Chu, X. Lv, J. Wu, J.-F. Li, Thermally stable piezoelectric properties of (K,Na)NbO_3-based lead-free perovskite with rhombohedral-tetragonal coexisting phase. Acta Mater. **122**, 344–351 (2017)
30. D. Wang, F. Hussain, A. Khesro, A. Feteira, Y. Tian, Q. Zhao, I.M. Reaney, Composition and temperature dependence of structure and piezoelectricity in $(1-x)(K_{1-y}Na_y)NbO_3$-$x(Bi_{1/2}Na_{1/2})ZrO_3$ lead-free ceramics. J. Am. Ceram. Soc. **100**, 627–637 (2017)
31. P. Ren, Z. Liu, M. Wei, L. Liu, J. Shi, F. Yan, H. Fan, G. Zhao, Temperature-insensitive dielectric and piezoelectric properties in $(1-x)K_{0.5}Na_{0.5}Nb_{0.997}Cu_{0.0075}O_3$-$xSrZrO_3$ ceramics. J. Eur. Ceram. Soc. **37**, 2091–2097 (2017)